JOURNAL OF MATERIALS SCIENCE **36** (2001) 4351–4360

Defect dynamics and damage of cement-based materials, studied by electrical resistance measurement

JINGYAO CAO, SIHAI WEN, D. D. L. CHUNG
Composite Materials Research Laboratory, State University of New York at Buffalo, Buffalo, NY 14260-4400, USA
E-mail: ddlchung@acsu.buffalo.edu

Defect dynamics, as studied by DC electrical resistance measurement during repeated compression of cement paste, mortar and concrete in the elastic regime, are characterized by defect generation that dominates during the first loading, defect healing that dominates during subsequent loading, and defect aggravation that dominates during subsequent unloading. The interface between sand and cement, that between silica fume and cement, and that between coarse aggregate and mortar contribute to the defect dynamics, particularly the defect healing. Electrical resistance measurement is also effective for monitoring damage, which causes the resistance to increase. Defect generation results in an irreversible increase in the baseline resistance as stress cycling progresses, whereas defect healing results in a reversible decrease in the resistivity upon compression within a stress cycle. Defect generation is relatively significant in the early cycles and diminishes upon cycling. As the cumulative damage increases, the extent of defect healing within a cycle also increases.

1. Introduction

Defects and damage affect the structural performance of cement-based materials, such as concrete. It is therefore important to monitor damage and understand how defects respond to mechanical stress or strain. This paper investigates both defect dynamics and damage of cement-based materials by electrical resistance measurement.

Defects greatly affect the properties of a material, so their control is of practical importance. Stress, heat and the environment all affect the defects, but this paper is focused on the effect of stress. Previous work on the effect of stress is mainly concerned with stress in the plastic deformation regime [1–5]. In the case of metals and polymer-matrix composites (such as asphalt), plastic deformation, particularly involving compression, can give rise to healing [1–5]. However, the effect of deformation is very different in the case of cement, due to the relatively brittle nature of cement. Plastic deformation of cement can lead to damage.

Stress application can generate defects, which may be a form of damage in a material. Stress application can also heal defects, particularly in the case of the stress being compressive. This healing is induced by stress and is to be distinguished from healing that is induced by liquids, chemicals or particles [6–16]. On the other hand, stress removal can aggravate defects, particularly in the case of the stress being compressive and the material being brittle. The generation, healing and aggravation of defects during dynamic loading are referred to as defect dynamics, which constitute one of the subjects of this paper. The little prior attention on defect dynamics is mainly due to the dynamic nature of defect healing and aggravation. For example, stress application can cause healing, and subsequent unloading can cancel the healing. This reversible nature of the healing makes the healing observable only in real time during loading. On the other hand, defect generation tends to be irreversible upon unloading, so it does not require observation in real time.

Observation in real time during loading is difficult for microscopy, particularly transmission electron microscopy, which is the type of microscopy that is most suitable for the observation of microscopic defects. However, observation in real time during loading can be conveniently performed by electrical measurement. As defects increase the electrical resistivity of a material, defect generation increases the resistivity whereas defect healing decreases the resistivity.

One objective of this paper is to use electrical resistivity measurement during repeated compressive loading and unloading to monitor the dynamics of defects. As stress affects the strain (i.e., the dimensions), which in turn affects the electrical resistance, this work involves simultaneous measurement of resistance and strain. In order to confirm the interpretation of the results in terms of defect dynamics, this work involves measurement of the resistivity in the stress direction (longitudinal resistivity) and that perpendicular to the stress direction (transverse resistivity).

Damage monitoring (i.e., structural health monitoring) is valuable for structures for the purpose of hazard mitigation. It can be conducted during the damage by acoustic emission detection. It can also be conducted after the damage by ultrasonic inspection, liquid penetrant inspection, dynamic mechanical testing or other techniques. Real-time monitoring gives information on the time, load condition or other conditions at which damage occurs, thereby facilitating the evaluation of the cause of the damage. Moreover, real-time monitoring provides information as soon as damage occurs, thus enabling timely repair or other hazard precaution measures. The second objective of this paper is to use electrical resistivity measurement to sense damage.

Fatigue in concrete is conventionally studied by destructive mechanical testing after different numbers of stress cycles. However, this method does not allow the monitoring of the progress of fatigue damage on the same specimen and is not very sensitive to minor damage. As different specimens can differ in the flaws, fatigue evolution is more effectively studied by monitoring one specimen throughout the fatigue process rather than interrupting the fatigue process at different times for different specimens. However, the monitoring of one specimen throughout the fatigue process requires a nondestructive method that is sensitive to minor damage. This paper shows that electrical resistivity measurement is effective for fatigue damage monitoring, particularly in the regime of minor damage, in addition to monitoring both defect generation and defect healing in real time.

Damage monitoring must be distinguished from strain sensing, as strain can be reversible and is not necessarily accompanied by damage. There has been considerable work on the use of electrical resistance measurement to sense strain in cement reinforced with short carbon fibers [17–24]. Compressive strain causes the resistance to decrease reversibly, whereas tensile strain causes the resistance to increase, due to fiber push-in during compression and fiber push-out during tension [17–20, 23, 24]. In contrast, this paper addresses the more basic case in which fibers are absent.

DC rather than AC resistance measurement was used in this work because of the relatively low equipment cost associated with DC measurement and the skin effect associated with AC measurement.

2. Experimental methods

2.1. Materials

This paper addresses three forms of cement-based materials, namely cement paste (without aggregate), mortar (with fine aggregate only) and concrete (with fine and coarse aggregates). Comparison of the results on cement paste and mortar allowed study of the effect of the interface between cement and fine aggregate. Comparison of the results on mortar and concrete allowed study of the effect of the interface between mortar and coarse aggregate.

2.1.1. Cement pastes

The cement used was portland cement (Type I) from Lafarge Corp. (Southfield, MI). The silica fume (Elkem Materials Inc., Pittsburgh, PA, microsilica EMS 965) was used in the amount of 15% by weight of cement. The latex, used in the amount of 20% by the weight of cement, was styrene butadiene copolymer (Dow Chemical Co., Midland, MI, 460NA) with the polymer making up about 48% of the dispersion and with styrene and butadiene in the weight ratio 66:34, such that the latex was used along with an antifoam (Dow Corning Corp., Midland, MI, #2410, 0.5% by weight of latex). Three types of cement paste were studied, namely (i) plain cement paste (consisting of just cement and water), (ii) silica-fume cement paste (consisting of cement, water and silica fume), and (iii) latex cement paste (consisting of cement, water, latex and antifoam). The water/cement ratio was 0.35 for pastes (i) and (ii), and was 0.23 for paste (iii). Six specimens of each of the three types of paste were tested.

A rotary mixer with a flat beater was used for mixing. Latex (if applicable) was mixed with the antifoam by hand for about 1 min. Then the latex mixture (if applicable), cement, water and silica fume (if applicable) were mixed in the mixer for 5 min. After pouring the mix into oiled molds, an external electric vibrator was used to facilitate compaction and decrease the amount of air bubbles. The specimens were demolded after 1 day and then allowed to cure at room temperature in air (relative humidity = 100%) for 28 days.

2.1.2. Mortars

The cement used was portland cement (Type I) from Lafarge Corp. (Southfield, MI). The sand used was natural sand (100% passing 2.36 mm sieve, 99.9% SiO_2). The sand/cement ratio was 1.0. Silica fume (Elkem Materials, Inc., Pittsburgh, PA, EMS 965) was used in the amount of 15% by weight of cement. A water reducing agent (WR) was used in the amount of 2.0% by weight of cement. The WR was TAMOL SN (Rohm and Haas, Philadelphia, PA) which contained 93–96% sodium salt of a condensed naphthalene sulfonic acid. The water/cement ratio was 0.35. No coarse aggregate was used. A Hobart mixer with a flat beater was used for mixing, which was conducted for 5 min. After that, the mix was poured into oiled molds. A vibrator was used to facilitate compaction and decrease the amount of air bubbles.

Two types of mortar were studied. They were (i) plain mortar (consisting of cement, sand, water and WR), and (ii) silica-fume mortar (consisting of cement, water, WR and silica fume). Six specimens of each type were tested.

2.1.3. Concrete

The cement used was portland cement (Type I) from Lafarge Corp. (Southfield, MI). Both fine and coarse aggregates were used. The fine aggregate was natural sand (99.9% SiO_2), 100% of which passed #8 U.S. sieve. The coarse aggregate was #57 (ASTM C33-84), 100% of which passed 25 mm (1 in) standard sieve. The ratio of cement to fine aggregate to coarse aggregate was 1:1.5:2.5.

The water-cement ratio was 0.45. A water-reducing agent (TAMOL SN, Rohm and Hass Co., Philadelphis, PA; sodium salt of a condensed naphthalenesulphonic acid) was used in the amount 2% of the cement mass.

All ingredients except water were mixed in a concrete mixer at a low speed for 1 min. After that, water was added and then mixing was conducted at a high speed for 5 min. After this, the concrete mix was poured into oiled cylindrical molds (125 mm diameter, 250 mm high). A vibrator was used to facilitate compaction and decrease the amount of air bubbles.

2.2. Testing

For compressive testing according to ASTM C109-80, cement paste and mortar speciments were prepared using a $2 \times 2 \times 2$ in ($51 \times 51 \times 51$ mm) mold. The strain was measured by using a strain gage attached to the middle of one of four side surfaces of a specimen. The strain gage was centered on the side surface and was parallel to the stress axis. Compressive testing under load control was performed using a hydraulic mechanical testing system (MTS Model 810). Testing was conducted either under repeated loading at various stress amplitudes or under cyclic loading. Cyclic loading was performed on mortar up to 100 cycles at a compressive stress amplitude of 34.5 MPa (compressive strain amplitude of 1.95×10^{-2}), such that each stress cycle (an isosceles triangle in the curve of stress vs. time and in the curve of strain vs. time within a cycle) took 20 s and the deformation was elastic (i.e., the strain was reversible).

During compressive testing of the cubes mentioned above, the longitudinal resistivity was measured using the four-probe method, in which silver paint in conjunction with copper wires served as electrical contacts. Four contacts were perimetrically around the specimen at four planes that were all perpendicular to the stress axis and that were symmetric with respect to the midpoint along the height of the specimen. The outer two contacts (typically 40 mm apart) were for passing current. The inner two contacts (typically 30 mm apart) were for measuring the voltage. A Keithley 2001 multimeter was used.

For concrete specimens, which were in the form of a cylinder, four electrical contacts in the form of silver pain in conjunction with copper wire strands were applied circumferentially around a cylindrical specimen for the purpose of electrical resistance measurement by the four-probe method. The outer two contacts (240 mm apart, symmetrically positioned relative to the center plane perpendicular to the cylindrical axis) were for passing current. The inner two contacts (230 mm apart, symmetrically positioned relative to the center plane perpendicular to the cylindrical axis) were for voltage measurement. A Keithley 2002 (Cleveland, OH) multimeter was used. Due to the larger diameter of the concrete cylinder, the current did not penetrate uniformly to the whole cross-section of a cylindrical specimen, as shown by the dependence of the measured resistivity on speciment size [25]. As a result, the resistivity was not determined for the case of concrete; only resistance on a relative scale was determined.

All specimens were allowed to air dry after removal from the moist curing chamber and before application of electrical contacts in the form of silver paint.

Compressive stress at a stress amplitude of 5.44 MPa (32.5% of the compressive strength, within the elastic regime) was applied to the top flat surface of a cylindrical specimen, while the resistance was measured. As a separate experiment, testing was conducted under repeated compressive loading at increasing stress amplitudes up to 5.44 MPa. A hydraulic mechanical testing system (MTS 810) was used to provide the stress under load control. Testing was conducted under cyclic loading up to 40 cycles, such that each stress cycle (an isosceles triangle in the curve of stress vs. time within a cycle) took 20 s.

Cement paste samples for transverse resistivity measurement were in the form of rectangular bars of size $150 \times 12 \times 11$ mm. Each electrical contact was applied around the entire 12×11 mm perimeter of the bar. The voltage contacts were at two parallel cross-sectional planes that were 40 mm apart. Thus, the resistivity was measured along the length of the rectangular bar. During the resistivity measurement, compressive stress was applied to the middle portion (19×12 mm) of the rectangular sample (Fig. 1), such that the electrical contacts were away from the stressed portion and the stress was in a direction perpendicular to the direction of resistivity measurement. The stress (repeated loading at increasing stress amplitudes) was provided by a hydraulic mechanical testing system (MTS Model 810). The transverse strain was measured using a strain gage attached to a side of the specimen, as shown in Fig. 1.

The resistivity was obtained from the resistance and the dimensions (both the length in the current direction and the cross-sectional area perpendicular to the current direction), which changed with the measured longitudinal strain and with the transverse strain resulting from the Poisson effect. However, neglecting the transverse strain affected the longitudinal resistivity value negligibly. The fractional change in resistance was essentially equal to the fractional change in resistivity.

Due to the voltage present during electical resistance measurement, electric polarization occurs as the resistance measurement is made continuously. The polarization results in an increase in the measured resistance, although the effect is only significant when the time of measurement is long, as in the case of fatigue

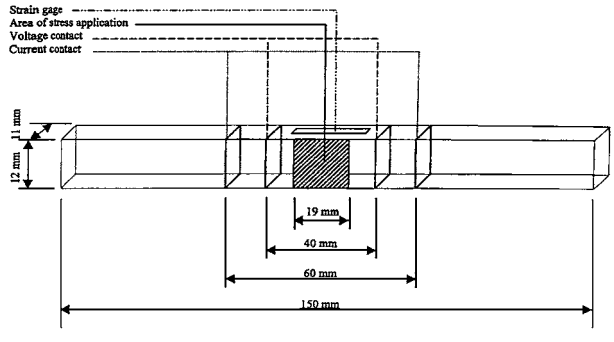

Figure 1 Sample configuration for measuring the transverse electrical resistivity during uniaxial compression.

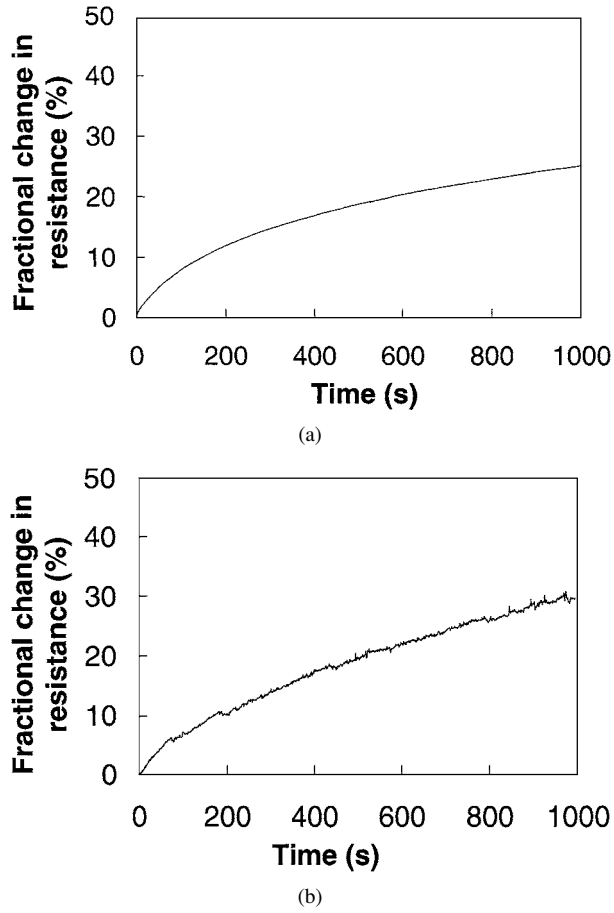

Figure 2 Fractional change in resistance vs. time of resistance measurement under no stress, (a) Plain mortar. (b) Plain concrete.

monitoring [3], and the effect diminishes in the presence of a compressive stress [26]. The polarization-induced resistance increase, as separately measured as a function of the time of resistance measurement in the absence of stress (Fig. 2a for mortar and Fig. 2b for concrete), was subtracted from the measured resistance change obtained during cyclic (fatigue) loading in order to correct for the effect of polarization. Due to the presence of a dynamic compressive stress in the resistance measurement of this work, the subtraction using the case without stress leads to inaccuracy in the resistance baseline during dynamic compression. In spite of this baseline inaccuracy, the effect of dynamic stress on the resistance is qualitatively meaningful.

The electrical resistivity is known to change with temperature [27], so the resistance baseline mentioned above is expected to shift with a change in temperature. Nevertheless, the qualitative effect of dynamic loading on the resistance is not expected to vary much with temperature, unless both stress and temperature vary dynamically at the same time.

In order to assess the extent of damage due to the cyclic loading, compressive testing involving static loading (at a loading rate of 0.287 MPa/s for mortar and 0.0604 MPa/s for concrete) up to failure was conducted before and after stress cycings (100 cycles for mortar and 40 cycles for concrete). Six specimens of each type were tested before cycling and six specimens of each type were tested after cycling.

3. Results and discussion

3.1. Defect dynamics

3.1.1. Cement paste

Fig. 3a shows the fractional change in longitudinal resistivity as well as the longitudinal strain during repeated compressive loading at an increasing stress amplitude. Fig. 3b shows the corresponding variation of stress and strain during the repeated loading. The strain varies linearly with the stress up to the highest stress amplitude (Fig. 3b). The strain returns to zero at the end of each cycle of loading. During the first loading, the fractional change in resistivity increases due to defect generation. During the subsequent unloading, the fractional change in resistivity continues to increase, due to defect aggravation (such as the opening of the microcracks generated during prior loading). During the second loading, the resistivity decreases slightly as the stress increases up to the maximum stress of the first cycle (due to defect healing) and then increases as the stress increases beyond this value (due to additional defect generation). During unloading in the second cycle, the resistivity increases significantly (due to defect aggravation, probably the opening of the microcracks). During the third loading, the resistivity essentially does not change (or decreases very slightly) as the stress increases to the maximum stress of the third cycle (probably due to the balance between defect generation

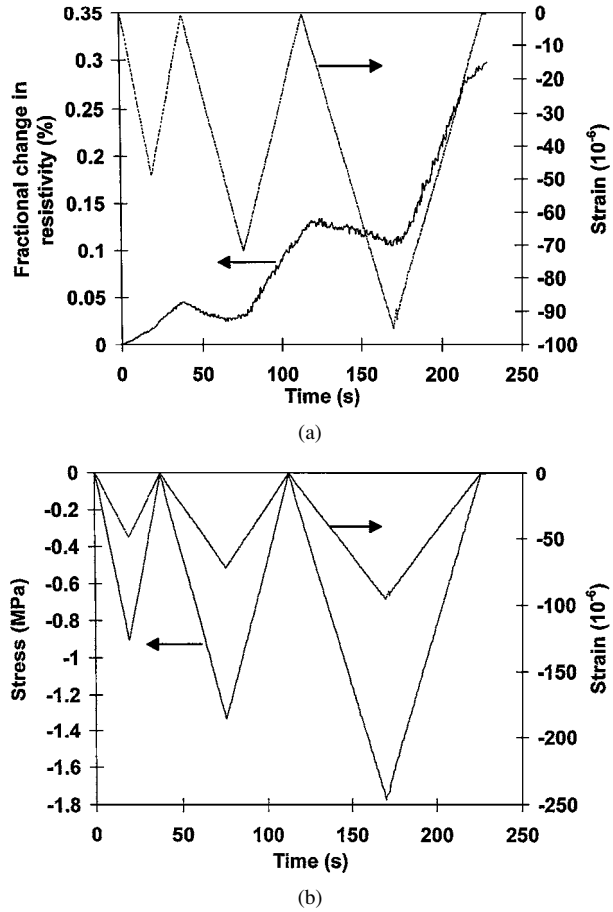

Figure 3 Variation of the fractional change in longitudinal resistivity with time (a), of the stress with time (b), and of the longitudinal strain (negative for compressive strain) with time (a, b) during dynamic compressive loading at increasing stress amplitudes within the elastic regime for plain cement paste.

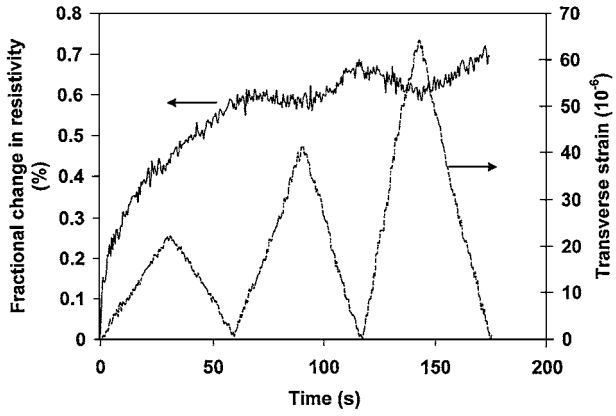

Figure 4 Variation of the fractional change in transverse resistivity with time and of the transverse strain with time during dynamic compressive loading at increasing stress amplitudes within the elastic regime for plain cement paste.

and defect healing). Subsequent unloading causes the resistivity to increase very significantly due to defect aggravation (probably the opening of the microcracks).

Fig. 4 shows the fractional change in transverse resistivity as well as the transverse strain (positive due to the Poisson effect) during repeated compressive loading at an increasing stress amplitude. The strain varies linearly with the stress and returns to zero at the end of each cycle of loading. During the first loading and the first unloading, the resistivity increases due to defect generation and defect aggravation respectively, as also shown by the longitudinal resistivity variation (Fig. 3). During the second loading, the resistivity first increases (due to defect generation) and then decreases (due to defect healing). During the second unloading, the resistivity increases, due to defect aggravation. During the third loading, the resistivity decreases due to defect healing. During the third unloading, the resistivity increases, due to defect aggravation.

The variations of the resistivity in the longitudinal and transverse directions upon repeated loading are consistent in showing defect generation (which dominates during the first loading), defect healing (which dominates during subsequent loading) and defect aggravation (which dominates during subsequent unloading). The defect aggravation during unloading follows the defect healing during loading, indicating the reversible (not permanent) nature of the healing, which is induced by compressive stress. The defect aggravation during unloading also follows the defect generation during loading.

In spite of the Poisson effect, similar behavior was observed in the longitudinal and transverse resistivities. This means that the defects mentioned above are essentially nondirectional and that the resistivity variations are real.

Comparion of Figs 3 and 4 shows that the increase in resistivity with strain during unloading in the second cycle is clear and less noisy for the longitudinal resistivity than the transverse resistivity. This suggests that defect aggravation is more significantly revealed by the longitudinal resistivity than the transverse resistivity. Hence, the defects are not completely non-directional.

Indentification of the defect type is beyond the scope of this paper. Microcracks were mentioned above just for the sake of illustration. The defects may be associated with certain heterogeneities in the cement paste.

Defects affect the mechanical properties. Therefore, mechanical testing (such as modulus measurement, which is nondestructive) can be used for studying defect dynamics. However, the modulus is not as sensitive to defect dynamics as the electrical resistivity, as shown in Fig. 3, where the relationship between stress and strain (Fig. 3b) is not affected while the resistivity (Fig. 3a) is affected. The low sensitivity of the modulus to defect dynamics is consistent with the fact that the deformation is elastic.

3.1.2. Mortars

Figs 5 and 6 show the variation of the fractional change in resistivity with cycle No. during initial cyclic compression of plain mortar and silica-fume mortar respectively. For both mortars, the resistivity increases abruptly during the first loading (due to defect generation) and increases further during the first unloading (due to defect aggravation). Moreover, the resistivity decreases during subsequent loading (due to defect healing) and increases during subsequent unloading

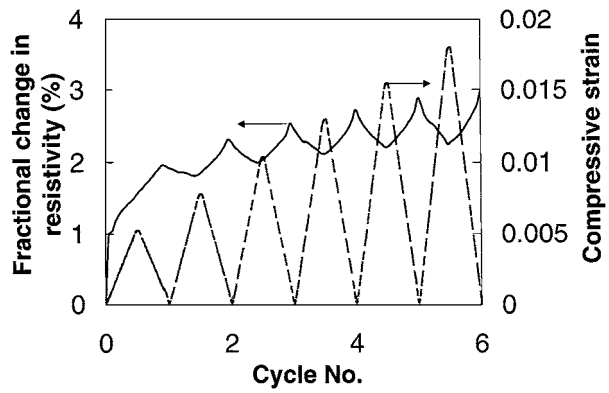

Figure 5 Variation of the fractional change in resistivity with Cycle No. (thick curve) and of the compressive strain with Cycle No. (thin curve) during repeated compressive loading at increasing stress amplitudes within the elastic regime for plain mortar.

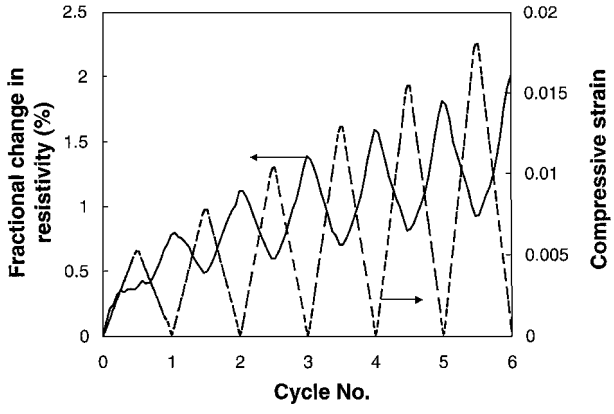

Figure 6 Variation of the fractional change in resistivity with Cycle No. (thick curve) and of the compressive strain with Cycle No. (thin curve) during repeated compressive loading at increasing stress amplitudes within the elastic regime for silica fume mortar.

(due to defect aggravation); the effect associated with defect healing is much larger for silica-fume mortar than for plain mortar. In addition, this effect intensifies as stress cycling at increasing stress amplitudes progresses for both mortars, probably due to the increase in the extent of minor damage. The increase in damage extent is also indicated by the resistivity baseline increasing gradually cycle by cycle. In spite of the increase in stress amplitude cycle by cycle, defect healing dominates over defect generation during loading in all cycles other than the first cycle.

Comparison of plain cement paste behavior (Section 3.1.1) and plain mortar behavior (this section) shows that the behavior is similar, except that the defect healing (i.e., the resistivity decrease upon loading other than the first loading) is much more significant in the mortar case. This means that the sand-cement interface in the mortar contributes significantly to the defect dynamics, particularly in relation to defect healing.

Comparison of Figs 5 and 6 shows that silica fume contributes significantly to the defect dynamics. The associated defects are presumably at the interface between silica fume and cement, even though this interface is diffuse due to the pozzolanic nature of silica fume. The defects at this interface are smaller than those at the sand-cement interface, but this interface is large in total area due to the small size of silica fume compared to sand.

3.1.3. Concrete

Fig. 7 shows the fractional change in resistance in the stress direction during repeated compressive loading at increasing stress amplitudes. The resistance increased during loading and unloading in Cycle 1, decreased during loading in all subsequent cycles and increased during unloading in all subsequent cycles. The higher the stress amplitude, the greater was the amplitude of resistance variation within a cycle.

The increase in resistance during loading in Cycle 1 is attributed to defect generation; that during subsequent unloading in Cycle 1 is attributed to defect aggravation. In all subsequent cycles, the decrease in resistance during loading is attributed to defect healing and the increase in resistance during unloading is attributed to defect aggravation.

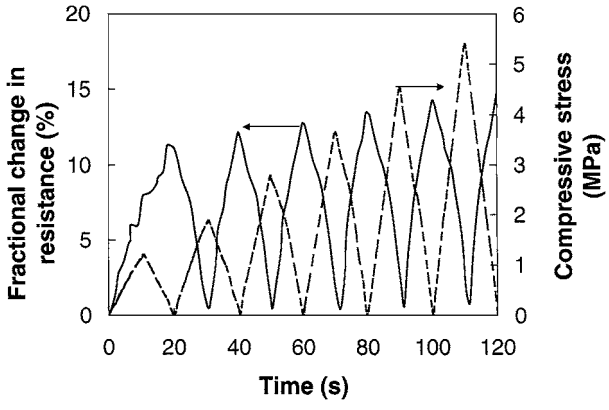

Figure 7 Fractional change in resistance (solid curve) and stress (dashed curve), both vs. time during repeated compressive loading at increasing stress amplitudes, for plain concrete.

The results of this section on concrete are consistent with those of Section 3.1.2 on mortar and those of Section 3.1.1 on cement paste. The compressive strength was higher for mortar than concrete. The defect dynamics, as indicated by the fractional change in resistance within a cycle, were more significant for concrete than mortar. The first healing, as indicated by the resistance decrease during loading in Cycle 2, was much more complete for concrete than mortar. These observations mean that the interface between mortar and coarse aggregate contributed to the defect dynamics (particularly healing), due to the interfacial voids and defects.

3.2. Damage

3.2.1. Cement pastes

Fig. 8a shows the fractional change in resistivity along the stress axis as well as the strain during repeated compressive loading at an increasing stress amplitude for plain cement paste. Fig. 8b shows the corresponding variation of stress and strain during the repeated loading. The strain varies linearly with the stress up to the highest stress amplitude (Fig. 8b). The strain does not return to zero at the end of each cycle of loading, indicating plastic deformation. In contrast, Section 3.1 is concerned with effects of elastic deformation.

The resistivity increases during loading and unloading in every loading cycle (Fig. 8a). The slope of the

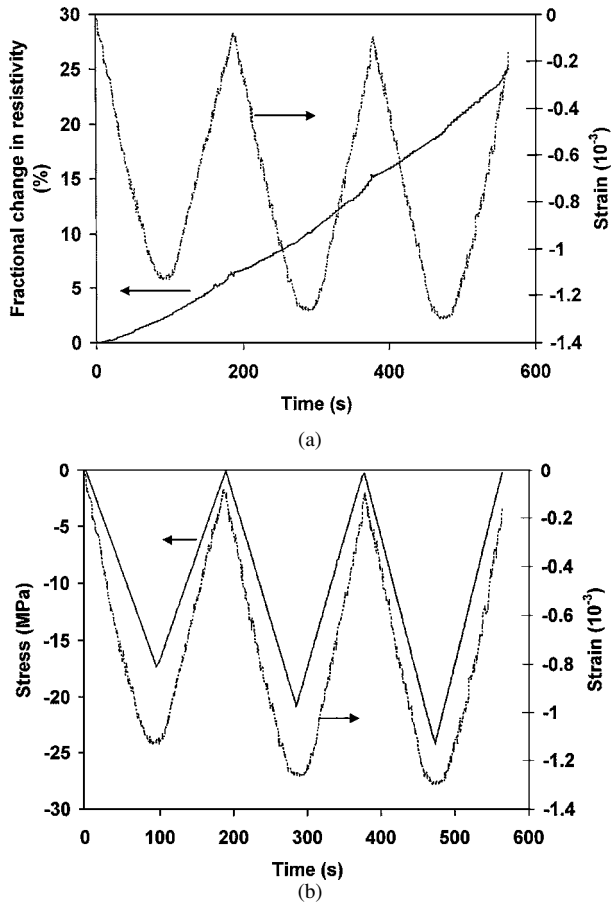

Figure 8 Variation of the fractional change in electrical resistivity with time (a), of the stress with time (b), and of the strain (negative for compressive strain) with time (a, b) during dynamic compressive loading at increasing stress amplitudes for plain cement paste.

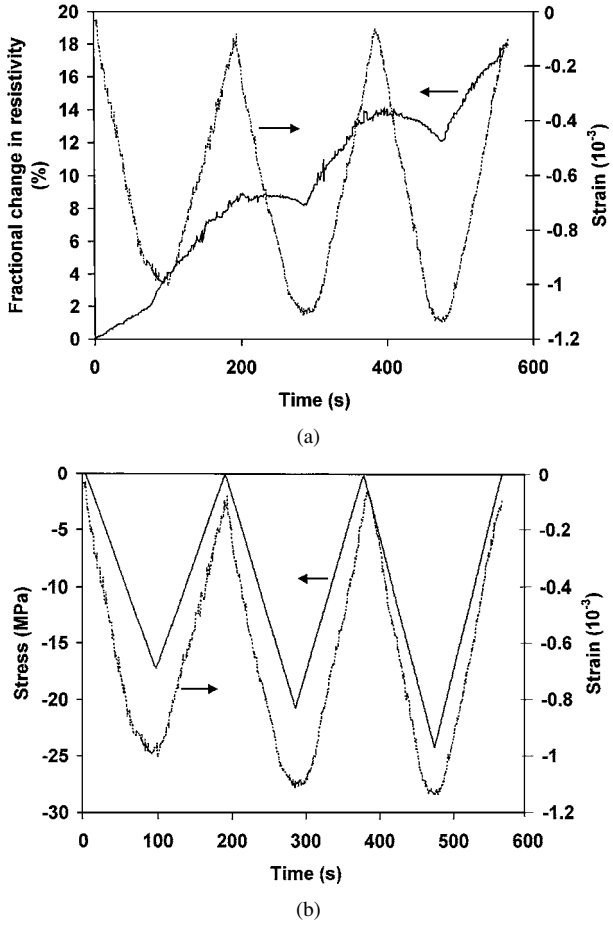

Figure 9 Variation of the fractional change in electrical resistivity with time (a), of the stress with time (b), and of the strain (negative for compressive strain) with time (a, b) during dynamic compressive loading at increasing stress amplitudes for silica-fume cement paste.

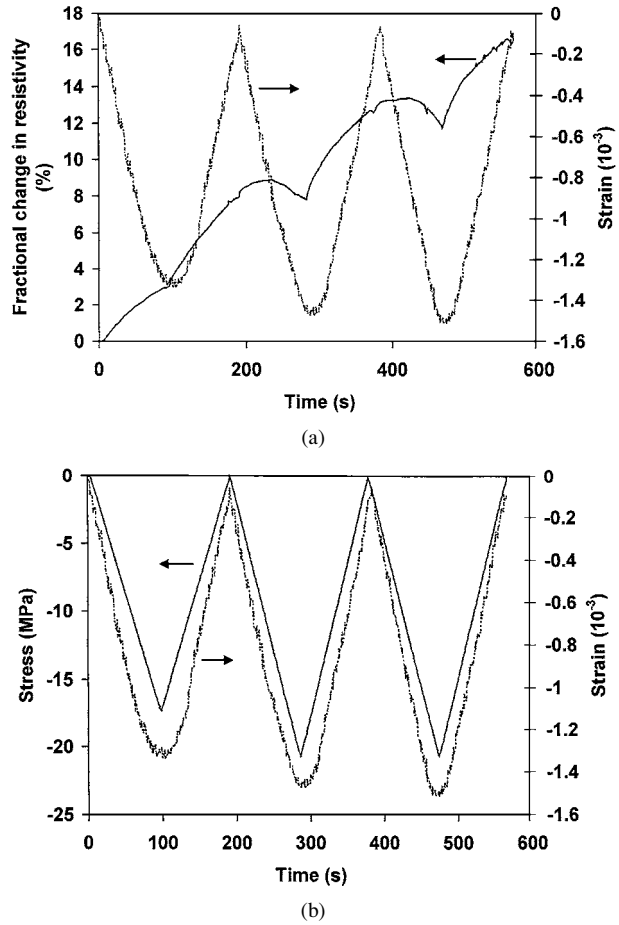

Figure 10 Variation of the fractional change in electrical resistivity with time (a), of the stress with time (b), and of the strain (negative for compressive strain) with time (a, b) during dynamic compressive loading at increasing stress amplitudes for latex cement paste.

curve of resistivity vs. time (Fig. 8a) increases with time, due to the increasing stress amplitude cycle by cycle (Fig. 8b) and the non-linear increase in damage severity as the stress amplitude increases. The resistivity increase during loading is attributed to damage infliction. The resistivity increase during unloading is attributed to the opening of microcracks generated during loading.

Fig. 9 gives the corresponding plots for silica-fume cement paste at the same stress amplitudes as Fig. 8. The strain does not return to zero at the end of each loading cycle, as in Fig. 8. The resistivity variation is similar to Fig. 8, except that the resistivity decreases during loading after the first cycle. The absence of a resistivity increase during loading after the first cycle is attributed to the lower tendency for damage infliction in the presence of silica fume, which is known to strengthen cement [28–31]. The resistivity decrease during loading after the first cycle is attributed to the partial closing of microcracks, as expected since the loading is compressive. In the absence of silica fume (i.e., plain cement paste, Fig. 8), the effect of damage infliction overshadows that of microcrack closing.

Fig. 10 gives the corresponding plots for latex cement paste. The resistivity effects are similar to those of Fig. 9a, except that the resistivity curve is less noisy and the rate of resistivity increase during first unloading is higher than that during first loading. This means that the microcrack opening during unloading has a larger effect on the resistivity than the damage infliction during loading.

Comparison of the results of this section for deformation in the plastic regime with those of Section 3.1.1 for deformation in the elastic regime shows that both the fractional change in resistivity and the strain are higher in this section than in Section 3.1.1 by orders of magnitude. Another difference is that the resistivity decreases are much less significant in this section than in Section 3.1.1. There is no resistivity decrease at all in Fig. 8a, but there are resistivity decreases in Fig. 3. These differences between the results of this section and of Section 3.1.1 are consistent with the much greater damage in plastic deformation than in elastic deformation and the tendency of damage to increase the resistivity.

That the resistivity decreases are not significant in the plastic deformation regime simplifies the use of the electrical resistivity to indicate damage. Nevertheless, even when the resistivity decreases are significant, the resistivity remains a good indicator of damage, which includes that due to damage infliction (during loading) and that due to microcrack opening. Microcrack closing, which causes the resistivity decreases, is a type of partial healing, which diminishes the damage. Hence, the resistivity indicates both damage and healing effects in real time.

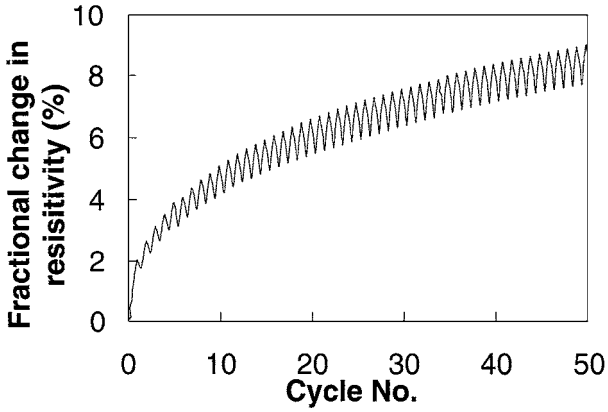

Figure 11 Fractional change in resistivity vs. compressive stress cycle number for Cycles 1–50 for plain mortar.

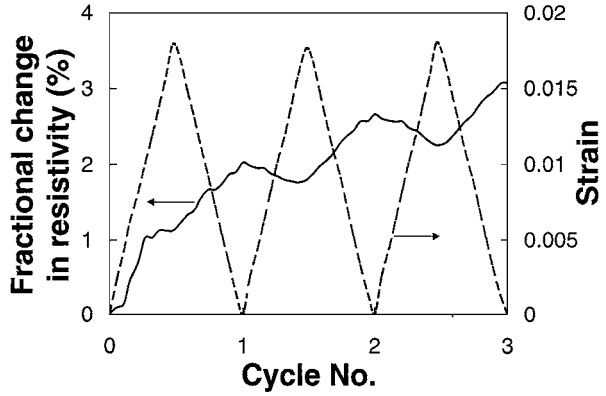

Figure 12 Fractional change in resistivity and strain, both vs. compressive stress cycle number for Cycles 1–3 for plain mortar.

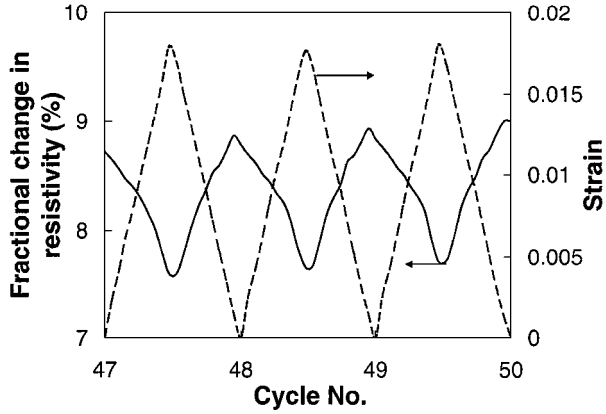

Figure 13 Fractional change in resistivity and strain, both vs. compressive stress cycle number for Cycles 48–50 for plain mortar.

3.2.2. Mortar

Figs 11–13 show the fractional change in resistivity in the stress direction versus cycle number during cyclic compression at a constant stress amplitude in the elastic regime (in contrast to the increasing stress amplitude in Section 3.2.1). Except for the first cycle, the resistivity decreases with increasing strain in each cycle and then increases upon subsequent unloading in the same cycle. As cycling progresses, the baseline resistivity continuously increases, such that the increase in quite abrupt in the first three cycles (Fig. 11) and that subsequent baseline increase is more gradual. In addition, as cycling progressed, the amplitude of resistivity decrease within a cycle gradually and continuously increases (Fig. 11).

The increase in baseline resistivity dominates the first cycle (Fig. 12) and corresponds to a fractional change in resistivity per longitudinal unit strain of -1.1 (negative because the strain was negative). This negative value suggests that the baseline resistivity increase is due to damage (defect generation). The baseline resistivity increase is irreversible, indicating the irreversibility of the damage. The incremental increase in damage diminishes as cycling progresses, as shown by the baseline resistivity increasing more gradually as cycling progresses.

The reversible decrease in resistivity within a stress cycle corresponds to a fractional change in resistivity per unit strain of $+0.72$ at cycle number 50 (Fig. 13). It is attributed to defect healing (reversible) under the compressive stress. As cycling progresses, the cumulative damage (as indicated by the baseline resistivity) increases and results in a greater degree of defect healing upon compression (hence, more decrease in resistivity within a cycle).

Both the baseline resistivity and the amplitude of resistivity decrease within a cycle serve as indicators of the extent of damage. Measurement of the baseline resistance does not need to be done in real time during loading, thus simplifying the measurement. However, its use in practice is complicated by possible shifts in the baseline by environmental, polarization and other factors. On the other hand, the measurement of the amplitude of resistivity decrease must be done in real time during loading, but it is not much affected by baseline shifts.

The compressive strength before stress cycling was 54.7 ± 1.7 MPa. That after 100 stress cycles was 53.1 ± 2.1 MPa. The modulus, as shown by the change of strain with stress in each cycle, was not affected by the cycling. Thus, the damage that occured during the stress cycling was slight, but was still detectable by resistivity measurement.

Comparison of the results of Section 3.1.1 on cement paste with those of this section on mortar shows that the fractional change in resistivity per unit strain (due to irreversible generation of defects in the elastic regime) is higher for mortar (1.1) than for cement paste (0.10). Moreover, comparison shows that mortar is more prone to defect healing (reversible) than cement paste, as expected from the presence of the interface between fine aggregate and cement in mortar.

3.2.3. Concrete

Figs 14–16 show the fractional change in resistance in the stress direction versus cycle number during cyclic compression at a constant stress amplitude. Except for the first cycle, the resistance decreased with increasing stress in each cycle and then increased upon subsequent unloading in the same cycle. As cycling progressed, the baseline resistivity gradually and irreversibly increased (Fig. 14). In addition, as cycling progressed, the amplitude of resistance decrease within a cycle gradually and continuously increased, especially in Cycles 1–9 (Fig. 14).

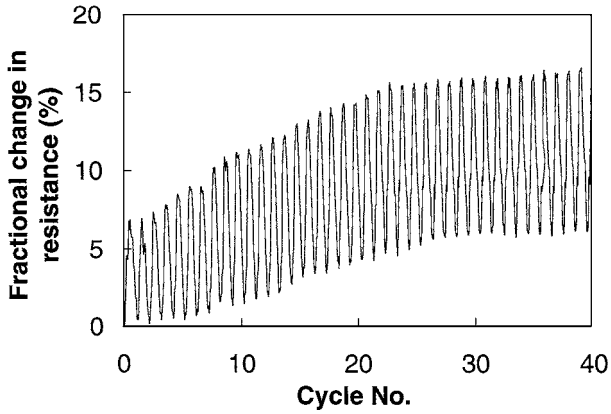

Figure 14 Fractional change in resistance vs. compressive stress cycle number for Cycles 1–40 for plain concrete.

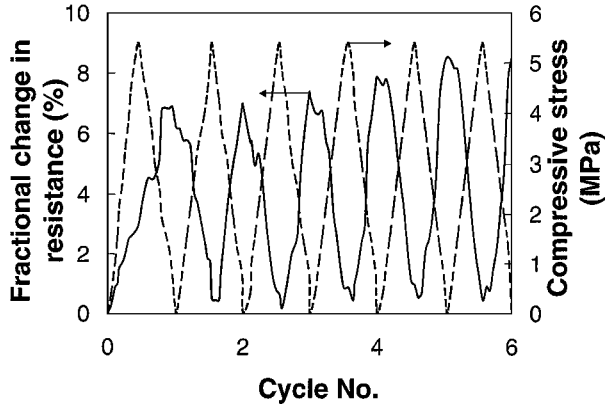

Figure 15 Fractional change in resistance (solid curve) and stress (dashed curve), both vs. compressive stress cycle number for Cycles 1–6 for plain concrete.

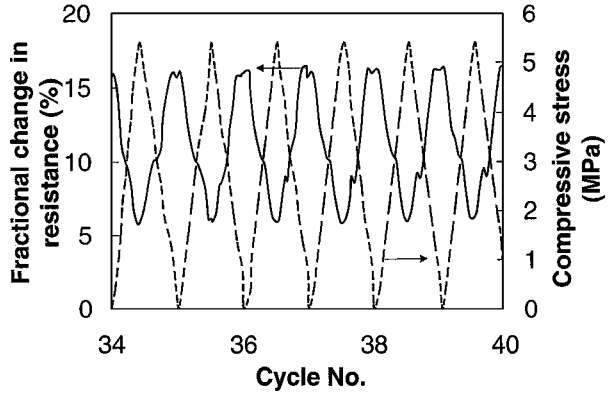

Figure 16 Fractional change in resistance (solid curve) and stress (dashed curve), both vs. compressive stress cycle number for Cycles 35–40 for plain concrete.

In the first cycle, the resistance increased upon loading and unloading, in contrast to all subsequent cycles, where the resistance decreased upon loading and increased upon unloading (Fig. 15).

The compressive strength before stress cycling was 16.73 ± 0.86 MPa. That after 40 stress cycles was 14.24 ± 0.97 MPa. Thus, the damage that occurred during the stress cycling was slight, but was still detectable by resistance measurement.

The gradual increase in baseline resistance as stress cycling progressed (Fig. 14) is attributed to irreversible and slight damage. The increase in the amplitude of resistance variation as cycling progressed (Fig. 14) is attributed to the effect of damage on the extent of defect dynamics. In other words, the more was the damage, the greater was the extent of defect healing during loading and the greater was the extent of defect aggravation during unloading.

The fractional loss in compressive strength after the cycling was greater for concrete than mortar, as expected from the higher compressive strength of mortar. Nevertheless, the baseline resistance increase was more significant for mortar than concrete, probably due to the relatively large area of the interface between cement and fine aggregate and the consequent greater sensitivity of the baseline resistivity to the quality of the interface between cement and fine aggregate than to the quality of the interface between mortar and coarse aggregate. In other words, the interface between cement and fine aggregate dominated the irreversible electrical effects.

4. Conclusion

Defect dynamics, as studied by electrical resistance measurement during repeated compressive loading of cement paste, mortar or concrete in the elastic regime, are characterized by (i) defect generation that dominates during the first loading, (ii) defect healing that dominates during subsequent loading, and (iii) defect aggravation that dominates during still subsequent unloading. Defect aggravation during unloading follows defect generation or defect healing during loading. Defect generation and aggravation cause the resistivity in both longitudinal and transverse directions to increase for cement paste; defect healing causes the resistivity in both directions to decrease.

The defects associated with both the interface between sand and cement and that between silica fume and cement respond in a dynamic fashion to repeated loading, thus contributing significantly to the defect dynamics of mortar, particularly in relation to defect healing. Similarly, the defects associated with the interface between coarse aggregate and mortar contribute to the defect dynamics of concrete particularly in relation to healing.

Damage monitoring of cement paste has been shown by electrical resistance measurement in the stress direction. For plain cement paste the resistance increases during compressive loading and unloading in every loading cycle due to damage infliction and microcrack opening respectively. For cement paste containing silica fume or latex, the resistance decreases slightly during loading after the first cycle due to microcrack closing, although the resistance increases during unloading in every cycle and during first loading. In general, the resistance indicates both damage (due to damage infliction and subsequent microcrack opening) and healing (due to microcrack closing) effects in real time.

Minor damage of mortar and concrete during cyclic compression in the elastic regime was monitored by measurement of the electrical resistance in the stress direction. The baseline resistivity (resistance in the case of concrete) irreversibly increases as cycling progresses

due to defect generation, which is most significant in the early cycles and diminishes as cycling progresses. Within a cycle, the resistivity (resistance in the case of concrete) decreases reversibly, due to defect healing upon compression. The amplitude of resistivity (resistance in the case of concrete) decrease in a cycle increases upon cycling, due to the increase in cumulative damage (indicated by the baseline resistivity or resistance) and the consequent increase in the extent of defect healing upon compression. Both the fractional increase in baseline resistivity (resistance) and the amplitude of resistivity (resistance) decrease in a cycle serve as indicators of damage.

References

1. E. S. HODGE, S. VISWANATHAN and T. W. REDDOCH, in Proceedings of the 1997 Automotive Alloys TMS Annual Meeting (Metals & Materials Soc (TMS), Warrendale, PA, 1997) p. 121.
2. Y. R. KIM, Y. C. LEE and H. J. LEE, *J. Mater. Civil Eng.* **7**(1) (1995) 59.
3. H. J. LEE and Y. R. KIM, *J. Eng. Mechanics-ASCE* **124**(11) (1998) 1224.
4. Y. KIM and Y. R. KIM, in Proceedings Engineering Mechanics (ASCE, New York, NY, 1996) Vol. 1, p. 612.
5. Y. R. KIM, S. L. WHITMOYER and D. N. LITTLE, *Transportation Research Record* (1454) (1994) 89.
6. H. CORDES and D. BICK, *Beton—und Stahlbetonbau* **86**(8) (1991) 181.
7. H. MEICHSNER, *Beton—und Stahlbetonbau* **87**(4) (1992) 95.
8. A. MOR, P. J. M. MONTEIRO and W. T. HESTER, *Cement, Concrete & Aggregates* **11**(2)(1989) 121.
9. C. EDVARDSEN, *Betonwerk und Fertigteil-Technik* **62**(11) (1996) 77.
10. S. JACOBSEN, J. MARCHAND and L. BOISVERT, *Cem. Concr. Res.* **26**(6) (1996) 869.
11. S. JACOBSEN and E. J. SELLEVOLD, *ibid.* **26**(1) (1996) 55.
12. S. JACOBSEN, J. MARCHAND and H. HORNAIN, *ibid.* **25**(8) (1995) 1781.
13. N. HEARN, *Materials & Structures* **31**(212) (1998) 563.
14. C. M. DRY, in Proceedings of the 3rd International Conference on Intelligent Materials and 3rd European Conference on Smart Structures and Materials, SPIE—the International Society for Optical Engineering (Society of Photo-Optical Instrumentation Engineers, Bellingham, WA, 1996) Vol. 2779, p. 958.
15. *Idem.*, in Proceedings of the 3rd International Conference on Intelligent Materials and 3rd European Conference on Smart Structures and Materials, SPIE—the International Society for Optical Engineering (Society of Photo-Optical Instrumentation Engineers, Bellingham, WA, 1996) Vol. 2719, p. 247.
16. C. DRY, *Smart Materials & Structures* **3**(2) (1994) 118.
17. X. FU, W. LU and D. D. L. CHUNG, *Carbon* **36**(9) (1998) 1337.
18. D. D. L. CHUNG, *Mater. Sci. Eng. Rev.* **22**(2) (1998) 57.
19. X. WANG, X. FU and D. D. L. CHUNG, *J. Mater. Res.* **14**(3) (1999) 790.
20. X. FU, W. LU and D. D. L. CHUNG, *Cem. Concr. Res.* **28**(2) (1998) 183.
21. X. FU and D. D. L. CHUNG, *ibid.* **27**(9) (1997) 1313.
22. X. FU, E. MA, D. D. L. CHUNG and W. A. ANDERSON, *ibid.* **27**(6) (1997) 845.
23. S. WEN and D. D. L. CHUNG, *ibid.* **31**(2) (2001) 297.
24. *Idem.*, *ibid.* **30**(8) (2000) 1289.
25. J. HOU and D. D. L. CHUNG, *Corrosion Sci.* **42**(9) (2) 1489.
26. S. WEN and D. D. L. CHUNG, *Cem. Concr. Res.* **31**(2) (2001) 291.
27. *Idem.*, *ibid.* **29**(6) (1999) 961.
28. Z. BAYASI and J. ZHOU, *ACI. Mater. J.* **90**(4) (1993) 349.
29. B. MA, J. LI and J. PENG, *J. Wuhan University of Technology, Materials Science Edition* **14**(2) (1999) 1.
30. K. TAN and X. PU, *Cem. Concr. Res.* **28**(12) (1998) 1819.
31. L. BAGEL, *ibid.* **28**(7) (1998) 1011.

Received 24 October 2000
and accepted 21 May 2001